Mining, Metallurgy & Exploration (2024) 41:669–680
https://doi.org/10.1007/s42461-024-00921-7

Full-Scale Demonstration and Performance Evaluation of a Hybrid Geopolymer/Biopolymer Cementitious Material Developed for Pumpable Roof Supports in Underground Mines

Arash Nikvar-Hassani[1,2] · **Timothy Batchler**[3] · **Lianyang Zhang**[1]

Received: 29 January 2023 / Accepted: 17 January 2024 / Published online: 6 February 2024

Abstract
Recently, a new hybrid geopolymer/biopolymer (GP/BP) cementitious material was developed for improving the performance of pumpable roof supports in underground mines. This study demonstrates the application of the hybrid GP/BP cementitious material and validates its effectiveness in full-scale. In this regard, eight (8) full-size (0.61 m diameter and 1.52 m height) cribs were produced in collaboration with Minova International Ltd and tested at the National Institute for Occupational Safety and Health (NIOSH) Mine Roof Simulator (MRS) Laboratory. These full-size cribs were produced with different material configurations to evaluate the effect of water to solid (W/S) ratio, Portland cement (PC) content, and BP dosage. The results demonstrated and validated the effectiveness of the hybrid GP/BP cementitious material in increasing the peak and residual bearing capacities of pumpable cribs and eliminating the issue of deterioration when exposed to air compared with the conventional Portland cement/fly ash (PC/FA) cementitious material currently used in practice. On average, the peak uniaxial compressive strength (UCS) and the highest residual UCS after peak of the full-size cribs produced from the hybrid GP/BP cementitious material are 1.90 and 1.33 times of those of the PC/FA-based full-size cribs by one company and 2.32 and 1.66 times of those of the PC/FA based full-size cribs by the other company, respectively.

Keywords Pumpable roof support · Fly ash · Portland cement · Geopolymer · Biopolymer · Ground control

1 Introduction

Effective roof support is critical to prevent ground falls and ground fall accidents. There are mainly two types of roof support systems, intrinsic supports, and standing supports. Intrinsic supports like roof bolts normally carry the load as roof deforms and interacts with the surrounding rock to reduce bed separation. On the other hand, standing supports take the load as roof and floor converges. Can support is probably the mostly widely used standing support which can provide large-deformation support. However, there are some limitations for Can support, including (i) wood chips required to provide a good contact with roof which decreases the efficiency of the support due to softening of the Can support and (ii) difficulty in handling and installation of the bulky supports [1–3].

To address the limitations of the conventional standing supports, pumpable roof supports (PRSs) are increasingly used [4]. A PRS contains a crib bag and the cementitious material in it (Fig. 1). To produce a PRS, the collapsible crib bag is hung to the roof and stretched down to the floor. Then, the bag is filled with a two stream cementitious material pumped from ground surface. The combination of the cured cementitious material with the confinement from crib bag with steel wires around it forms the complete PRS.

For a PRS to provide effective and safe support to the roof, the key is to ensure that the support system, especially the cementitious material, to have high peak and residual strength and be stable with time through the mining induced loading [7, 8]. However, the cementitious material currently used in practice to produce PRSs is conventional Portland cement/fly ash (PC/FA) based and has limitations, including (1) the peak and residual bearing capacities are inconsistent and sometimes too small and (2) when exposed to the air, the PC/FA based cementitious

✉ Arash Nikvar-Hassani
nikvar@arizona.edu

✉ Lianyang Zhang
lyzhang@arizona.edu

[1] Department of Civil and Architectural Engineering and Mechanics, The University of Arizona, Tucson, AZ, USA

[2] Power and Dams, Stantec, Denver, United States

[3] CDC NIOSH, Pittsburgh, PA, USA

material severely deteriorates, potentially rendering the support much weaker and adversely affecting the overall safety [3]. To enhance the performance of PRSs, an unconventional cementitious material that can effectively minimize or alleviate the limitations of the conventional PC/FA cementitious material needs to be developed.

In this regard, we recently developed a new cementitious material based on a novel cement called geopolymer (GP) for enhancing the performance of PRSs [3]. GP is a class of cementitious material that is formed by alkali or acid activation of high aluminosilicate content precursors [9–18]. Compared with the conventional PC, GP not only shows superior performance like rapid strength gain and low shrinkage but also consumes less energy and produces lower greenhouse gas emissions [19–21]. Like the conventional PC, however, GP also shows brittle behavior with low fracture toughness. Therefore, we used biopolymer (BP) to improve the ductility of the GP cementitious material [22–24]. The underlying mechanism for this improvement is that the BP dissolved in the activator solution creates thin films around the unreacted particles and creates a bridge between cracks, enhancing the mechanical properties of the GP [24, 25].

For convenient mining applications where the material is typically pumped from the surface to the active mine section underground where the support is constructed, the new hybrid GP/BP cementitious material was designed to be a mixture of two pumpable grout streams (Fig. 2). Stream 1 is composed of FA, cement kiln dust (CKD) or PC, superplasticizer (SP) and water, and stream 2 contains sodium hydroxide (SH), sodium silicate (SS), and BP. The FA is the aluminosilicate source for GP formation. The CKD or PC is for adjusting and controlling the setting time of the hybrid cementitious material while the SP is for improving the pumpability of stream 1. The SH is the alkali activator for GP formation and the SS is for adjusting the Si/Al ratio and providing additional Na+ cations for charge balancing. The BP (e.g., carrageenan) is for further enhancing the mechanical behavior of the GP through formation of an interpenetrating cross-linked network binding and toughening the GP matrix [3, 26]. When the two streams stay alone, they remain as a slurry and a solution, respectively, and can be easily handled and transported. When they are mixed together and poured into a crib bag through a Y-connector, a GP/BP composite cementitious material is formed. The new hybrid GP/BP cementitious material can be tailored and used in practice at different conditions to achieve the optimum performance by simply adjusting the relative amount of the different components [24].

The hybrid GP/BP cementitious material has been successfully developed for improving the performance of PRSs in the laboratory [24]. As a preliminary demonstration and validation, small-size (0.15 m diameter and 0.30 m height) bagged specimens were produced and tested. The results clearly show that the bagged specimen produced from the hybrid GP/BP cementitious material has much higher peak and residual strength than the crib bagged pumpable roof supports currently used in practice [2].

Before the hybrid GP/BP cementitious material based PRSs are applied in practice, their performance and effectiveness need to be demonstrated and validated in a full scale. Therefore, full-size pumpable cribs were produced and tested to demonstrate and validate the effectiveness of the hybrid GP/BP cementitious material in a field scale. Specifically, eight (8) full-size (0.61 m diameter and 1.52 m height) cribs were produced in collaboration with Minova International Ltd and tested at the National Institute for Occupational Safety and Health (NIOSH) Mine Roof Simulator (MRS) Laboratory. These full-size pumpable cribs were produced using the hybrid GP/BP cementitious material at different conditions in order to evaluate the effect of water to solid (W/S) ratio, PC content, and BP dosage. The results will be useful for commercialization of the hybrid GP/BP cementitious material for practical applications. This paper presents the full-scale tests performed and the results obtained.

2 Production and Test of Full-Size Pumpable Cribs

2.1 Materials

The materials used for producing the pumpable cribs include class F fly ash (FA), ordinary Portland cement

Fig. 1 **a** Crib bag in a collapsed configuration hung to the roof; and **b** crib bag after filling with cementitious material [5, 6]

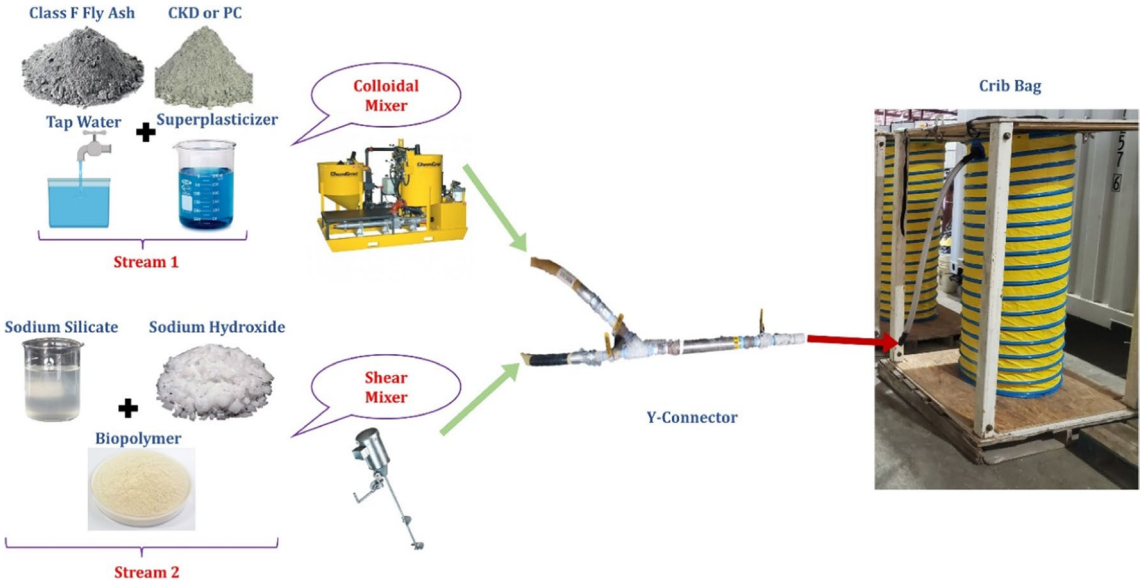

Fig. 2 Flow chart of two grout streams pumped to a crib bag to form pumpable roof support

(PC), reagent grade 98% sodium hydroxide (SH) (NaOH), sodium silicate (SS) (Na_2SiO_3) solution, superplasticizer (SP), biopolymer (BP), and tap water. The FA is the aluminosilicate source for geopolymer (GP) formation and was purchased from Eco-Material Technologies in Cadiz, OH. The PC type I/II is a high calcium content material selected as an accelerator to adjust and control the setting time of the hybrid cementitious material and was obtained from Argos S.A. cement company through a local supplier. Table 1 shows the chemical composition of the FA and PC from XRF analysis. The FA contains mainly silica and alumina while the PC contains mainly calcite and silica. The NaOH is an alkali activator required for GP formation and was purchased from Chemical Store in Clifton, NJ. The SS solution (SiO_2 = 28.00–29.74%, Na_2O = 8.70–9.38%, and H_2O = 60.88–63.3%) is for adjusting the Si/Al ratio and providing additional Na^+ cations for charge balancing and was purchased from Hawkins Inc in Roseville, MN. The SP is for adjusting and controlling the pumpability of the first stream and was purchased from Sika Corporation, California. The BP (carrageenan, CAR) was used to further enhance the mechanical behavior of the GP. The CAR is a natural high molecular weight polysaccharide produced from seaweed plant [27] and was obtained from Ingredion Inc., Westchester, IL.

2.2 Methodology

The hybrid GP/BP cementitious material is designed to be a mixture of two separate pumpable grout streams: stream 1 composed of FA, PC, SP, and water and stream 2 containing SH, SS, BP, and water (Fig. 2). To prepare the first stream, the FA, PC, and water were first mixed in a ChemGrout 600 high pressure colloidal mixer (Fig. 3), and then the SP was added while mixing continued to obtain a homogeneous slurry. To prepare the second stream, the SS solution was first placed in a container, and then SH pellets were dissolved in it and left at room temperature to cool down before used. When BP was used, it was also added at the same time as the SH in order to be thoroughly mixed in the solution. After both streams were ready, they were pumped through two separate pipes and then mixed through a Y-connector and poured into the crib bag (Fig. 4). The crib bags filled with the hybrid cementitious material (Fig. 5) were kept at room temperature for 28 days and then transported to the NIOSH MRS laboratory for testing. During the production of the full-size (0.61 m diameter and 1.52 m height) cribs, small-size (76.2 mm diameter and 152.4 mm height) unbagged specimens were also produced for evaluating the mechanical properties of the hybrid cementitious material itself.

In total, eight (8) full-size cribs were produced aiming to study the effect of main factors: water to solid (W/S) ratio

Table 1 Chemical composition of FA and PC

Chemical compound	SiO_2	Al_2O_3	CaO	Fe_2O_3	MgO	Na_2O	SO_3	K_2O	LOI	Others
FA (wt. %)	49.92	27.64	2.45	12.48	0.76	0.79	1.29	2.38	2.90	1.11
PC (wt. %)	19.4	4.8	62.2	3.0	2.8	0.69	3.1	NA	4.01	NA

Fig. 3 ChemGrout 600 high pressure colloidal mixer used for mixing and pumping stream 1

(0.55, 0.60), PC content (20, 30 wt.% of FA + PC), and BP dosage (0, 0.3 wt.% of FA + PC). Two cribs were produced at each condition. The details of the eight cribs are shown in Table 2. For all the cribs, SP at a dosage of 2 wt.% of FA + PC was used in stream 1, and a SH concentration of 5 M and a SS/SH ratio of 1 were selected for stream 2.

The uniaxial compression tests were conducted using the NIOSH MRS loading machine (Fig. 6) at a constant loading rate of 0.5 in/min (0.21 mm/s) to measure the peak uniaxial compressive strength (UCS) and the residual UCS of the cribs. The small-size unbagged cylinder specimens were tested using a Humboldt compression machine at a loading rate of 0.25 MPa/sec to measure the peak UCS of the hybrid GP/BP cementitious material with no crib bag confinement.

Fig. 4 Y-connection used to mix stream 1 and stream 2

Fig. 5 Crib bags filled with hybrid cementitious material

Scanning electron microscopy (SEM) imaging was performed in the SE conventional mode with a FEI INSPECT-S equipped with a Thermo Noran 6 energy-dispersive X-ray spectroscopy (EDX) detector to investigate the microstructure of the hybrid GP/BP cementitious material at different conditions. The fresh surface of failed specimens from the uniaxial compression tests, without polishing to keep the fractured surface "un-contaminated," were used for the SEM imaging. Along with the SEM, EDX was also conducted to evaluate the elemental composition of the hybrid GP/BP cementitious material. The XRD analysis was also done using a X'Pert Pro MPD X-ray diffractometer (Philips Analytical) equipped with the Cu Ka X-ray source and real-time multiple strip (RTMS) X'celerator detector. The XRD patterns were recorded within the range of 2 theta angles from 5° to 90°, with the rate of about 1.9°/min. The sample composition analysis was performed using the X'Pert HighScore software (Philips Analytical).

3 Results and Discussion

3.1 Small-Size Unbagged Cylinder Specimens

Figure 7 shows the peak UCS of the small-size unbagged cylinder specimens produced during the production of the full-size cribs. As can be seen, by increasing the BP content from 0 wt.% to 0.3 wt.% at W/S = 0.55 and 0.60, the peak UCS increased from 5.38 to 6.11 MPa and from 8.36 to 11.11 MPa, respectively. The peak UCS at W/S = 0.60 is higher than that at W/S = 0.55 mainly because a higher

Table 2 Eight full-size cribs produced using the hybrid cementitious materials at different conditions

Number of cribs	Composition of hybrid cementitious material					
	W/S	PC content (wt.% of FA + PC)	BP content (wt.% of FA + PC)	SP content (wt.% of FA + PC)	SH concentration	SS/SH
2	0.55	20	0	2	5 M	1
2	0.55	20	0.3	2	5 M	1
2	0.60	30	0	2	5 M	1
2	0.60	30	0.3	2	5 M	1

Fig. 6 NIOSH MRS loading machine used to test the full-size cribs

PC content (30 wt.% instead of 20 wt.%) was used at the higher W/S ratio.

3.2 Full-Size Cribs

3.2.1 Effect of SH Concentration and SS/SH Ratio

Figure 8 shows the stress–strain curves of the full-size cribs produced from the hybrid GP/BP cementitious material with W/S = 0.55 and 20 wt.% PC and at 0 wt.% BP (Fig. 8a) and 0.3 wt.% BP (Fig. 8b), respectively. For comparison, the stress–strain curves of the full-size cribs from Company I and Company II with the conventional PC/FA cementitious material currently used in practice are also shown in Fig. 8. As can be seen, the full-size cribs produced from the hybrid GP/BP cementitious material have much higher peak UCS and slightly higher or about the same residual UCS compared with the full-size cribs from Company I and Company II with the conventional PC/FA cementitious material currently used in practice. Table 3 provides a summary of the peak UCS, the highest residual UCS after peak, the strain at the peak stress, and the number of shed events obtained from the stress–strain curves in Fig. 8. As can be seen, the addition of 0.3 wt.% BP improved the mechanical performance of the cribs. For example, by including 0.3 wt.% BP, the peak UCS increased from 7.46 to 8.64 MPa, although the highest residual UCS after peak slightly decreased from 5.00 to 4.80 MPa. Also, by including 0.3 wt.% BP, the strain at the peak stress increased from 3.31 to 3.96% and the number of shed events decreased from 4 to 3. This is probably because the shrinkage/micro-cracking was reduced during the drying process by creating thick and high tensile biopolymer dehydrates like films between the particles [24, 25, 28].

Figure 9 shows the stress–strain curves of the cribs produced from the hybrid GP/BP cementitious material with W/S = 0.60 and 30 wt.% PC, and at 0 wt.% BP (Fig. 9a) and 0.3 wt.% BP (Fig. 9b), respectively. Again, for comparison, the stress–strain curves of the full-size cribs from Company

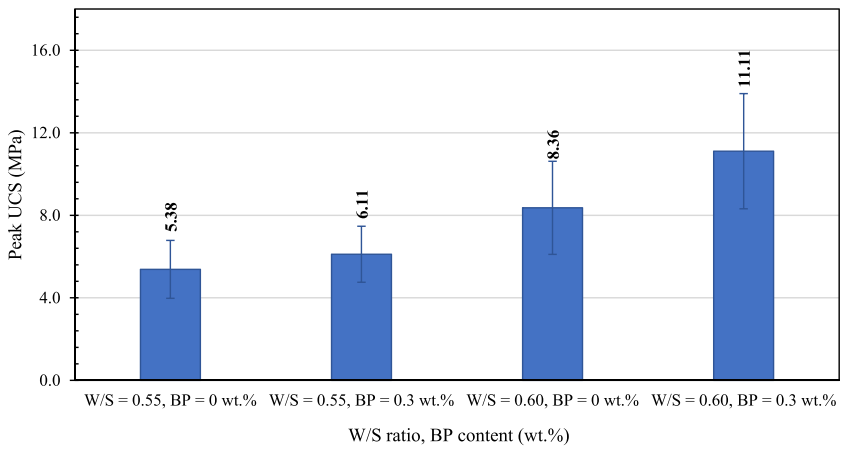

Fig. 7 Peak UCS of small-size (76.2 mm height and 152.4 mm in diameter) unbagged cylinder specimens produced from the hybrid GP/BP cementitious material during the production of full-size cribs

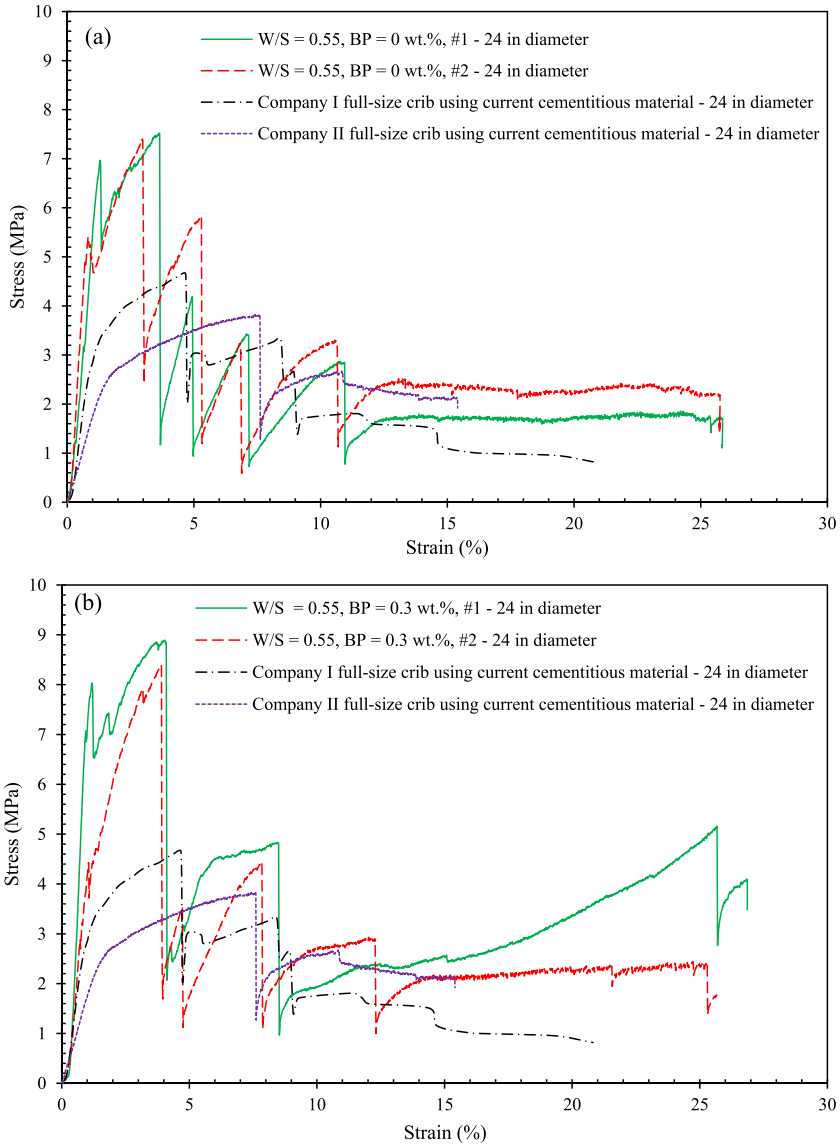

Fig. 8 Stress–strain curves obtained from uniaxial compression test of full-size cribs produced from the hybrid GP/BP cementitious material with W/S = 0.55 and 20 wt.% PC at **a** 0 wt.% BP, and **b** 0.3 wt.% BP

I and Company II with the conventional PC/FA cementitious material currently used in practice are also shown in Fig. 9. As can be seen, the full-size cribs produced from the hybrid GP/BP cementitious material have much higher peak UCS and slightly higher or about the same residual UCS compared with the full-size cribs from Company I and Company II with the conventional PC/FA cementitious material currently used in practice. Table 4 provides a summary of the peak UCS, the highest residual UCS after peak, the strain at the peak stress, and the number of shed events obtained

Table 3 Summary of results obtained from the stress–strain curves of full-size cribs produced from the hybrid GP/BP cementitious material with W/S = 0.55 and 20 wt.% PC at different BP contents

Crib	Peak UCS (MPa)	Average peak UCS (MPa)	Highest residual UCS after peak (MPa)	Average highest residual UCS after peak (MPa)	Strain at peak stress (%)	Average strain at peak stress (%)	Number of shed events	Average number of shed events
W/S = 0.55, BP = 0 wt.%, #1	7.39	7.46	4.17	5.00	2.97	3.31	4	4
W/S = 0.55, BP = 0 wt.%, #2	7.52		5.83		3.65		4	
W/S = 0.55, BP = 0.3 wt.%, #1	8.89	8.64	5.16	4.80	4.04	3.96	2	3
W/S = 0.55, BP = 0.3 wt.%, #2	8.38		4.43		3.89		4	

from the stress–strain curves in Fig. 9. As can be seen, the peak UCS slightly decreased from 10.02 MPa at 0 wt.% BP to 9.17 MPa at 0.3 wt.% BP. However, the highest residual UCS after peak increased from 3.33 MPa at 0 wt.% BP to 4.56 MPa at 0.3 wt.% BP. Also, the strain at the peak stress increased from 1.56% at 0 wt.% BP to 2.53% at 0.3 wt.% BP. This is probably due to the increase in fracture toughness of the hybrid cementitious material by the added BP [22].

Figure 10 compares the peak UCS of the small-size unbagged cylinder specimens and the full-size cribs produced from the hybrid GP/BP cementitious material at different W/S ratios and BP contents. Overall, the full-size cribs tend to have higher peak UCS than the small-size unbagged cylinder specimens simply because the crib bag with the steel wires provides confinement to the cementitious material.

3.3 Microstructural Analysis

SEM imaging and EDX analysis were conducted to investigate the effect of W/S ratio and BP dosage on the microstructure and elemental composition of the hybrid GP/BP cementitious material. Figure 11 shows the SEM micrographs and EDX spectra of the hybrid GP/BP cementitious material at two different BP contents and with the same W/S = 0.55 and 20 wt.% PC and cured at room temperature for 28 days. Due to the low dosage of BP, the microstructure of both specimens (0 wt.% and 0.3 wt.% BP) is similar, although more cracks can be seen in the specimen with 0 wt.% BP. The formation of cracks is due to the fast setting and curing at the presence of PC [29]. The sponge-like geopolymer gels and the calcium silicate hydrate (CSH) gels that act as the binder can be clearly seen. The formation of CSH gels is due to the presence of PC as a high calcium content material in the

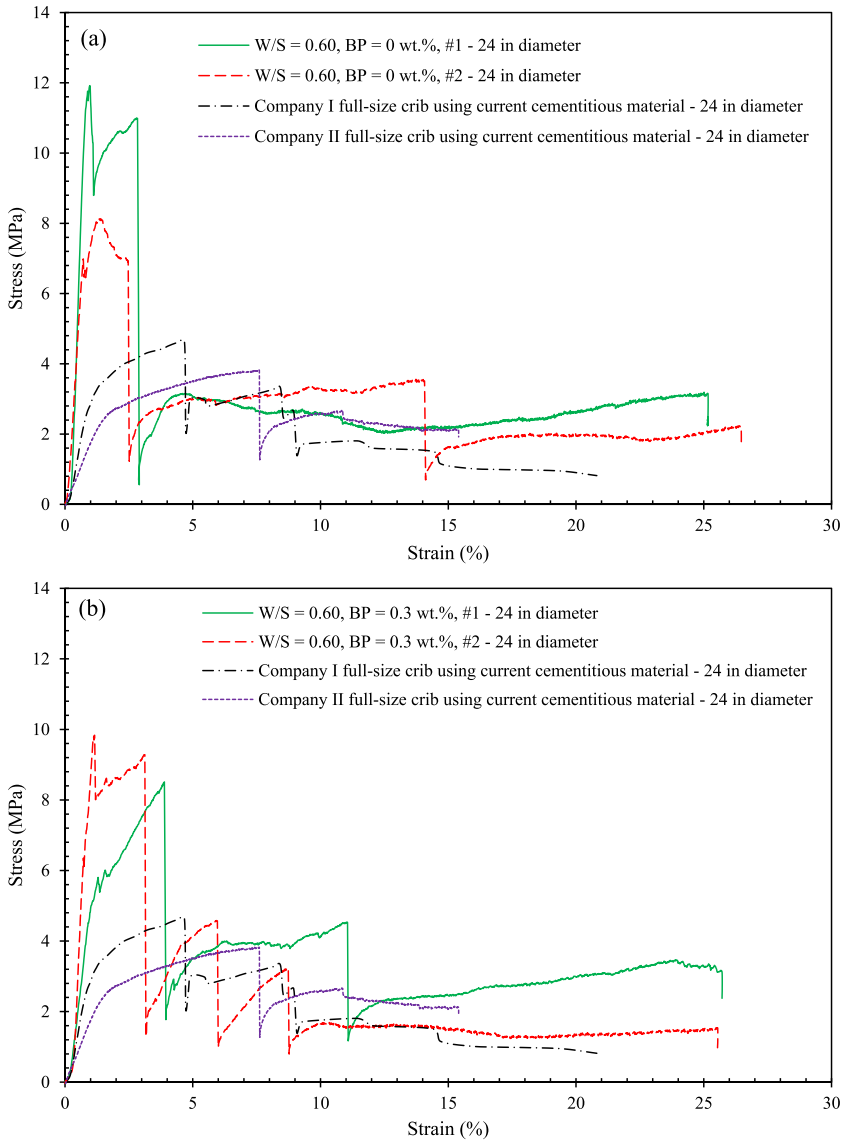

Fig. 9 Stress–strain curves obtained from uniaxial compression test of full-size cribs produced from the hybrid GP/BP cementitious material with W/S = 0.60 and 30 wt.% PC at **a** 0 wt.% BP, and **b** 0.3 wt.% BP

Table 4 Summary of results obtained from stress–strain curves of full-size cribs produced from the hybrid GP/BP cementitious material with W/S = 0.60 and 30 wt.% PC at different BP contents

Crib	Peak UCS (MPa)	Average peak UCS (MPa)	Highest residual UCS after peak (MPa)	Average highest residual UCS after peak (MPa)	Strain at peak stress (%)	Average strain at peak stress (%)	Number of shed events	Average number of shed events
W/S = 0.60, BP = 0 wt.%, #1	11.92	10.02	3.11	3.33	0.97	1.56	2	2
W/S = 0.60, BP = 0 wt.%, #2	8.12		3.55		1.34		2	
W/S = 0.60, BP = 0.3 wt.%, #1	8.51	9.17	4.53	4.56	3.89	2.53	2	3
W/S = 0.60, BP = 0.3 wt.%, #2	9.83		4.58		1.16		4	

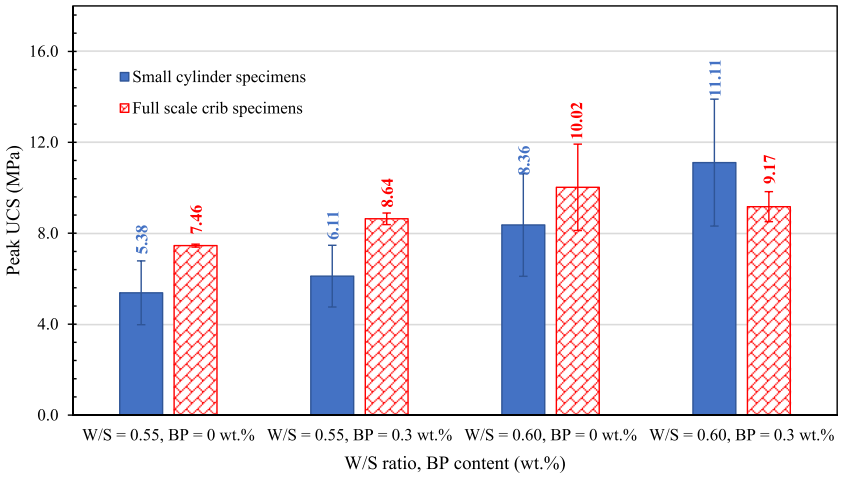

Fig. 10 Peak UCS of small-size unbagged cylinder specimens and full-size cribs produced from the hybrid GP/BP cementitious material at different W/S ratios and BP contents

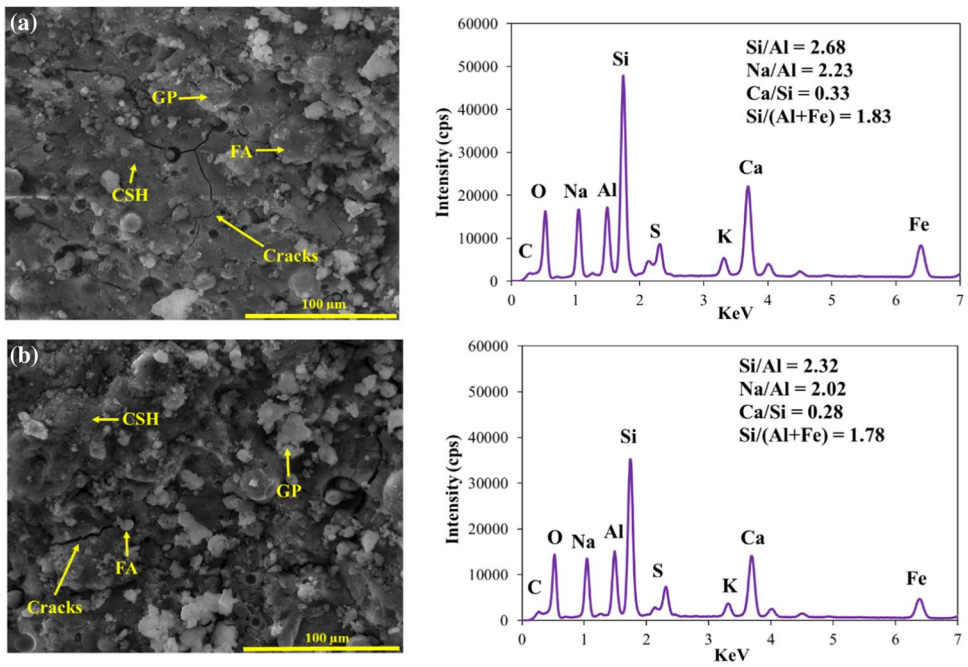

Fig. 11 SEM micrographs and EDX spectra of hybrid GP/BP cementitious material at W/S = 0.55, 20 wt.% PC, and with **a** 0 wt.% BP and **b** 0.3 wt.% BP

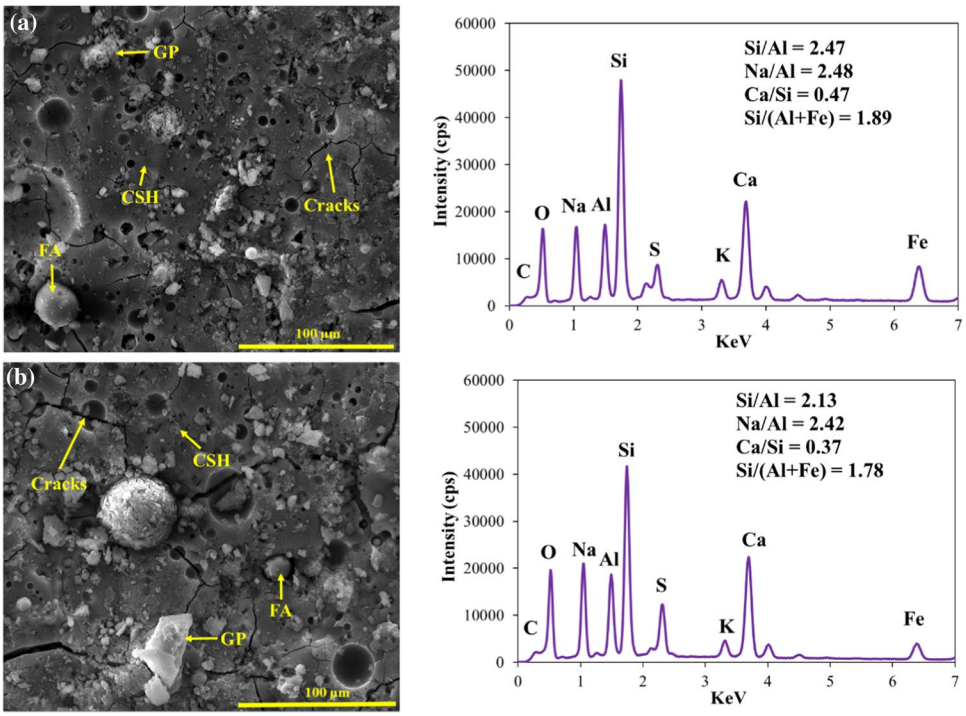

Fig. 12 SEM micrographs and EDX spectra of hybrid GP/BP cementitious material produced at W/S = 0.60, 30 wt.% PC, and with **a** 0 wt.% BP and **b** 0.3 wt.% BP

hybrid GP/BP cementitious material [30, 31]. Some unreacted or partially reacted FA particles can also be clearly seen, which may be due to the low alkalinity (5 M NaOH) used in preparing the cementitious material. Also, due to the low dosage of BP, the element compositions of the two hybrid cementitious materials (0 wt.% and 0.3 wt.% BP) are similar.

Figure 12 shows the SEM micrographs and EDX spectra of the hybrid GP/BP cementitious material at two different BP contents (0 wt.% and 0.3 wt.% BP) and with the same W/S = 0.60 and 30 wt.% PC and cured at room temperature for 28 days. By comparing Figs. 11 and 12, more cracks can be seen in the specimens in Fig. 12. This is simply because

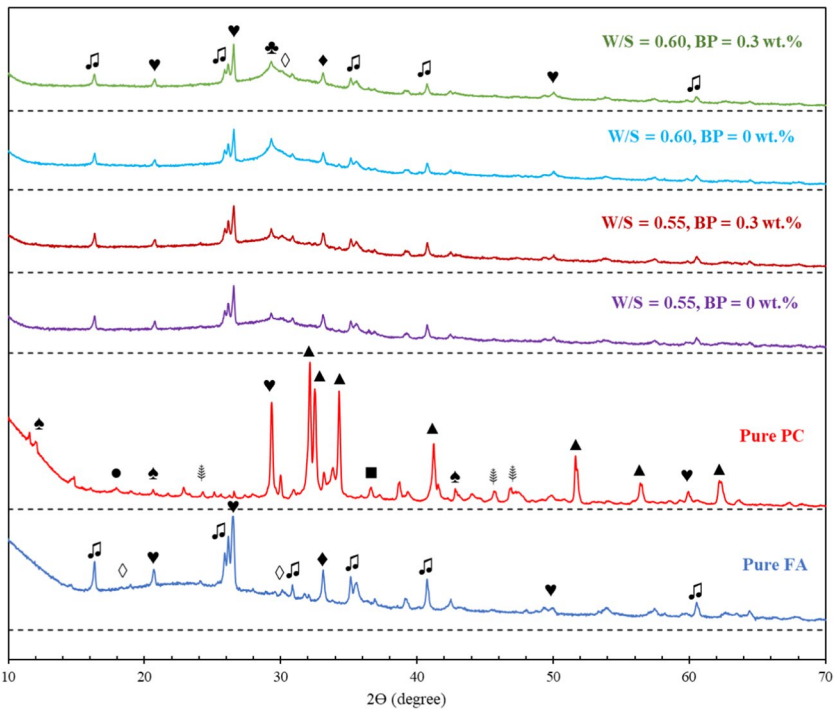

Fig. 13 XRD patterns of pure fly ash, PC, and GP/BP specimens at different W/S ratios and BP contents. Legend: ♠: gypsum ($(CaSiO_4)_2H_2O$), ▲:C_3S (Ca_3SiO_5), ♥: quartz (SiO_2), ♣: Calcite ($CaCO_3$), ♦: hematite (Fe_2O_3), ●:calcium hydroxide ($Ca(OH)_2$), ■: magnesium (Mg),⋕: brownmillerite ($Ca_2(Al,Fe)_2O_5$), ♫: mullite ($3Al_2O_3{\cdot}2SiO_2$), ◇: calcium aluminate ($CaAl_2O_4$)

Table 5 Comparison of peak UCS and highest residual UCS after peak of the full-size cribs produced from the hybrid GP/BP cementitious material at different conditions and those of the full-size cribs from Company I and Company II using conventional PC/FA cementitious material

Crib	Peak UCS (MPa) (divided by Company I value; divided by Company II value)	Highest residual UCS after peak (MPa) (divided by Company I value; divided by Company II value)
Hybrid cementitious material at W/S = 0.55, and BP = 0 wt.%	7.46 (1.60; 1.96)	5.00 (1.50; 1.88)
Hybrid cementitious material at W/S = 0.55, and BP = 0.3 wt.%	8.64 (1.86; 2.27)	4.80 (1.44; 1.80)
Hybrid cementitious material at W/S = 0.60, and BP = 0 wt.%	10.02 (2.15; 2.63)	3.33 (1.00; 1.25)
Hybrid cementitious material at W/S = 0.60, and BP = 0.3 wt.%	9.17 (1.97; 2.41)	4.56 (1.37; 1.71)
Company I – PC/FA based	4.65	3.33
Company II – PC/FA based	3.81	2.66

more PC (30 wt.% instead of 20 wt.%) was included and a quicker setting and curing occurred [29]. Also, because more PC (30 wt.% instead of 20 wt.%) was used, the Ca/Si ratios increased.

Figure 13 shows the XRD patterns of the hybrid GP/BP specimens prepared at different W/S ratios with 0 and 0.3 wt.% BP. The XRD patterns of the pure fly ash and PC are also provided for comparison. As can be seen, the XRD patterns of the GP/BP specimens are very similar to that of pure fly ash indicating that partly reacted fly ash particles are the main constituent of the geopolymer matrix. A broad hump between 10° and 40° indicates the amorphous phase produced during geopolymerization. With the addition of PC, a new peak "calcite" is formed which is attributed to the calcium silicate hydrate (CSH) gel, and it is the product of hydration reaction of the PC. The intensity of the calcite peak is higher for the specimens prepared at W/S = 0.60 compared with the specimens prepared at W/S = 0.55

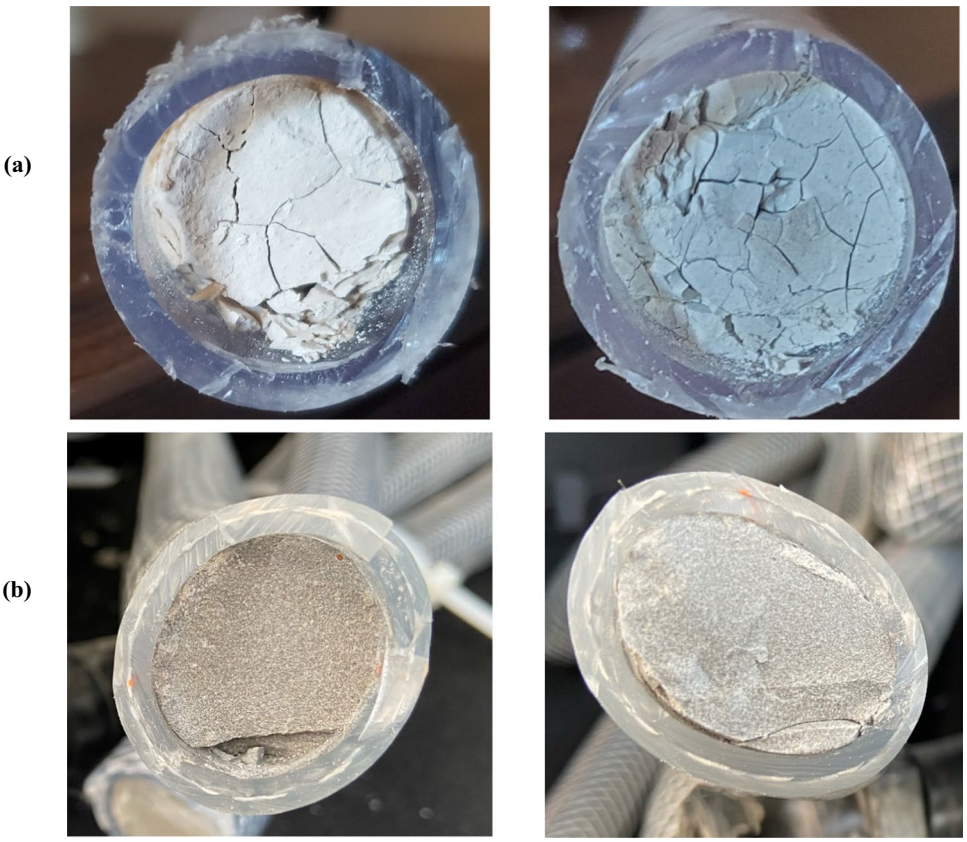

Fig. 14 Exposed cementitious material one day after cutting the pumping tubes connected to full-size pumpable cribs: **a** PC/FA-based cementitious material (with many cracks formed) and **b** hybrid GP/BP cementitious material (with no crack formed)

mainly due to the higher PC content (30 wt.% instead of 20 wt.%) used for the production of the GP/BP specimens at the higher water content. The addition of BP did not have a noticeable impact on the XRD patterns, probably due to the very low dosage used.

3.4 Technology Capability Assessment

The full-size crib test results demonstrated and validated the effectiveness of the hybrid GP/BP cementitious material in increasing both the peak and residual bearing capabilities of pumpable cribs compared to the PC/FA cementitious material currently used in practice. As shown in the summary Table 5, on average, the peak UCS and the highest residual UCS after peak of the full-size cribs produced from the hybrid GP/BP cementitious material are 1.90 and 1.33 times of those of the Company I full-size cribs and 2.32 and 1.66 times of those of the Company II full-size cribs, respectively. It is noted that since all the full-size cribs use similar crib bags, the increase in bearing capacity is mainly due to new hybrid GP/BP cementitious material.

The full-size crib production and tests also proved that the hybrid GP/BP cementitious material can successfully avoid the air degradation problem of the conventional PC/FA cementitious material (see Fig. 14). This is probably due to the higher degree of drying shrinkage in the PC/FA based cementitious material. The high level of shrinkage and consequently cracking of the PC based binder with SS additive due to drying is reported in the literature [32, 33]. The SS here is used as a quick setting agent which results in rapid settling of cement particles before gelation and thus much free water left in the pores [32]. However, for the hybrid GP/BP cementitious material, the SS is used to provide sufficient Si to form the GP and the very little excess water is ionized (salted) and thus no cracking due to drying shrinkage happens.

4 Conclusions

The production and tests of full-size cribs clearly demonstrated and validated the superior behavior of the new hybrid GP/BP cementitious material for enhancing the performance of pumpable roof supports. Compared with the conventional PC/FA cementitious material currently used in practice, the hybrid GP/BP cementitious material can increase both the peak and residual bearing capacities of pumpable roof supports and effectively eliminate the deterioration of the cementitious material when exposed to the air. However, due to the limited budget, only a small number of full-size cribs were produced and tested. Before applying the new hybrid GP/BP cementitious material to produce pumpable roof supports in practice, it is recommended more full-size cribs are produced and tested to further validate its performance.

Acknowledgements The authors would like to thank Minova International Ltd for their great support during the production and tests of the full-size cribs. Especially, Fred Cybulski, Field Services Lead, and Jason Tinsley, General Manager of Field Services, were very supportive and helpful in planning and producing the pumpable roof supports. The funding received from Alpha Foundation for the Improvement of Mine Safety and Health, Inc. (Alpha Foundation) for this project is greatly appreciated. The views, opinions, and recommendations expressed herein are solely those of the authors and do not imply any endorsement by the Alpha Foundation, its Directors and staff.

Data Availability All data and models generated or used during the study appear in the submitted article.

Declarations

Conflict of Interest The authors declare no competing interests.

References

1. Peng SS (2000) Cutting through open entries require proper support. Coal Age 6:37–40
2. TM Barczak (2005) An overview of standing roof support practices and developments in the United States. In: Best practices in rock engineering, proceedings of the third southern african rock engineering symposium, 10 - 12 October, 2005. Johannesburg, Republic of South Africa: South African Institute of Mining and Metallurgy, pp 301–334
3. Nikvar-Hassani A, Zhang L (2022) Synthesis of a CKD modified fly ash based geopolymer cementitious material for enhancing pumpable roof support. Mater Struct Constr 55. https://doi.org/10.1617/s11527-022-01899-8
4. Mark C, Barczack TM (2000) Proceedings: new technology for coal mine roof support. In: New Technology for Coal Mine Roof Support. Cincinnati, OH: U.S. Department of Health and Human Services, Public Health Service, Centers for Disease Control and Prevention, National Institute for Occupational Safety and Health, DHHS (NIOSH), pp 23–42
5. Jennmar Corporation (2013) J-CRIB pumpable crib catalogue. Taken from "www.jennchem.com.au"
6. NTI (2019) Pumpable cribs. NTI Min tunneling Co
7. Barczak TM, Tadolini SC (2008) Pumpable roof supports : an evolution in longwall roof support technology. Trans Soc Mining, Metall Explor 324:19–31
8. Batchler T (2017) Analysis of the design and performance characteristics of pumpable roof supports. Int J Min Sci Technol 27:91–99. https://doi.org/10.1016/j.ijmst.2016.10.003
9. Davidovits J (2008) Geopolymer chemistry & application. Institute Géopolymèr, F-02100 Saint-Quentin, France
10. Duxson P, Fernández-Jiménez A, Provis JL et al (2007) Geopolymer technology: the current state of the art. J Mater Sci 42:2917–2933. https://doi.org/10.1007/s10853-006-0637-z
11. Provis JL (2014) Geopolymers and other alkali activated materials: why, how, and what? Mater Struct Constr 47:11–25. https://doi.org/10.1617/s11527-013-0211-5
12. Zhuang XY, Chen L, Komarneni S et al (2016) Fly ash-based geopolymer: clean production, properties and applications. J Clean Prod 125:253–267. https://doi.org/10.1016/j.jclepro.2016.03.019
13. Majidi B (2009) Geopolymer technology, from fundamentals to advanced applications: a review. Mater Technol 24:79–87. https://doi.org/10.1179/175355509X449355
14. Xiaolong Z, Shiyu Z, Hui L, Yingliang Z (2021) Disposal of mine tailings via geopolymerization. J Clean Prod 284:124756. https://doi.org/10.1016/j.jclepro.2020.124756

15. Guo H, Yuan P, Zhang B et al (2021) Realization of high-percentage addition of fly ash in the materials for the preparation of geopolymer derived from acid-activated metakaolin. J Clean Prod 285:125430. https://doi.org/10.1016/j.jclepro.2020.125430
16. Louati S, Baklouti S, Samet B (2016) Acid based geopolymerization kinetics: effect of clay particle size. Appl Clay Sci 132–133:571–578. https://doi.org/10.1016/j.clay.2016.08.007
17. Lin H, Liu H, Li Y, Kong X (2021) Properties and reaction mechanism of phosphoric acid activated metakaolin geopolymer at varied curing temperatures. Cem Concr Res 144:106425. https://doi.org/10.1016/j.cemconres.2021.106425
18. Wei Q, Liu Y, Le H (2022) Mechanical and thermal properties of phosphoric acid activated geopolymer materials reinforced with mullite fibers. Materials (Basel) 15. https://doi.org/10.3390/ma15124185
19. Turner LK, Collins FG (2013) Carbon dioxide equivalent (CO2-e) emissions: a comparison between geopolymer and OPC cement concrete. Constr Build Mater 43:125–130. https://doi.org/10.1016/j.conbuildmat.2013.01.023
20. Manjarrez L, Nikvar-Hassani A, Shadnia R, Zhang L (2019) Experimental study of geopolymer binder synthesized with copper mine tailings and low-calcium copper slag. J Mater Civ Eng 31:04019156. https://doi.org/10.1061/(ASCE)MT.1943-5533.0002808
21. Van Deventer JS, Provis J, Duxson P, Lukey GC (2006) Technological environmental and commercial drivers for the use of geopolymers in a sustainable material industry. In: International symposium of advanced processing of metals and materials, pp 241–52
22. Li Z, Chen R, Zhang L (2013) Utilization of chitosan biopolymer to enhance fly ash-based geopolymer. J Mater Sci 48:7986–7993. https://doi.org/10.1007/s10853-013-7610-4
23. Li Z, Zhang L (2016) Fly ash-based geopolymer with kappa-carrageenan biopolymer. Biopolym Biotech Admixtures Eco-Efficient Constr Mater 173–192. https://doi.org/10.1016/B978-0-08-100214-8.00009-9
24. Nikvar-Hassani A, Zhang L (2022) Development of a biopolymer modified geopolymer based cementitious material for enhancement of pumpable roof support. Mater Struct Constr 55:1–22. https://doi.org/10.1617/s11527-022-01953-5
25. Chang I, Im J, Cho G-C (2016) Geotechnical engineering behaviors of gellan gum biopolymer treated sand. Can Geotech J 53:1658–1670. https://doi.org/10.1139/cgj-2015-0475
26. Nikvar-Hassani A, Zhang L (2020) Development of a new geopolymer based cementitious material for pumpable roof supports in underground mining. Geo-Congress 2020: Engineering, Monitoring, and Management of Geotechnical Infrastructure. American Society of Civil Engineers, Reston, VA, pp 325–334
27. Dul M, Paluch KJ, Kelly H et al (2015) Self-assembled carrageenan / protamine polyelectrolyte nanoplexes — investigation of critical parameters governing their formation and characteristics. Carbohydr Polym 123:339–349. https://doi.org/10.1016/j.carbpol.2015.01.066
28. Nakamatsu J, Kim S, Ayarza J et al (2017) Eco-friendly modification of earthen construction with carrageenan: water durability and mechanical assessment. Constr Build Mater 139:193–202. https://doi.org/10.1016/j.conbuildmat.2017.02.062
29. Mehta A, Siddique R (2017) Properties of low-calcium fly ash based geopolymer concrete incorporating OPC as partial replacement of fly ash. Constr Build Mater 150:792–807. https://doi.org/10.1016/j.conbuildmat.2017.06.067
30. Ahmari S, Zhang L (2013) Utilization of cement kiln dust (CKD) to enhance mine tailings-based geopolymer bricks. Constr Build Mater 40:1002–1011. https://doi.org/10.1016/j.conbuildmat.2012.11.069
31. Nath P, Sarker PK (2015) Use of OPC to improve setting and early strength properties of low calcium fly ash geopolymer concrete cured at room temperature. Cem Concr Compos 55:205–214. https://doi.org/10.1016/j.cemconcomp.2014.08.008
32. Yu Z, Yang L, Zhou S et al (2018) Durability of cement-sodium silicate grouts with a high water to binder ratio in marine environments. Constr Build Mater 189:550–559. https://doi.org/10.1016/j.conbuildmat.2018.09.040
33. Wang S, He C, Nie L, Zhang G (2019) Study on the long-term performance of cement-sodium silicate grout and its impact on segment lining structure in synchronous backfill grouting of shield tunnels. Tunn Undergr Sp Technol 92:103015. https://doi.org/10.1016/j.tust.2019.103015